SCIENCE CHINA
Technological Sciences

•Article•

October 2021 Vol.64 No.10: 2246–2254
https://doi.org/10.1007/s11431-020-1896-5

An efficient chemical reduction-induced assembly of Fe_3O_4@graphene fiber for wire-shaped supercapacitors with ultrahigh volumetric energy density

XIAO Peng[1,5], SHI MinJie[2*], XU Li[3], TAO FengBo[1], LI Yu[4], ZHU HangTian[2], LIU YuTing[2], LI ZhiMin[2], ZHOU YunPeng[2] & FENG Wei[4*]

[1] *State Grid Jiangsu Electric Power Co. Ltd. Research Institute, Nanjing 211103, China;*
[2] *School of Materials Science and Engineering, Jiangsu University of Science and Technology, Zhenjiang 212003, China;*
[3] *State Key Laboratory of Advanced Transmission Technology, Global Energy Interconnection Research Institute Co. Ltd., Beijing 102211, China;*
[4] *School of Materials Science and Engineering, Tianjin University, Tianjin 300354, China;*
[5] *Institute of Functional Nano & Soft Materials (FUNSOM), Jiangsu Key Laboratory for Carbon-Based Functional Materials & Devices, Soochow University, Suzhou 215213, China*

Received January 12, 2021; accepted July 5, 2021; published online August 19, 2021

Benefiting from high flexibility and weavability, the wire-shaped supercapacitors (SCs) arouse tremendous interests for the applications in wearable/portable electronics. Graphene fiber (GF) is considered as a promising linear electrode for wire-shaped SCs. However, the bottleneck is how to develop the GF-based linear electrode with facile fabrication process while well-maintaining satisfactory electrochemical performance. Herein, a novel Fe_3O_4@GF composite linear electrode is proposed via a chemical reduction-induced assembly approach, in which the GO and Fe_3O_4 nanoparticles (NPs) realize the efficient self-assembly owing to the electrostatic and van der Waals interactions, as well as the sufficient reduction of GO during the preparation process. The resultant fiber-shaped architecture shows boosted charge-transfer kinetics, high flexibility and structural integrity. Such Fe_3O_4@GF linear electrode exhibits excellent electrochemical behaviors including a large volumetric specific capacitance (~250.75 F cm^{-3}), remarkable rate capability and favorable electrochemical kinetics in aqueous electrolyte, superior than previously reported GF-based linear electrodes. For real application, a high-performance wire-shaped SC with excellent flexibility and weavability is fabricated based on such Fe_3O_4@GF linear electrode and gel electrolyte, demonstrating ultrahigh volumetric energy density (18.8 mWh cm^{-3}), power density (4000 mW cm^{-3}) and strong durability (~93.5% retention after 10000 cycles). Prospectively, the fabricated wire-shaped SC can maintain reliable electrochemical behaviors in various deformation states, showing its potentials in future portable and wearable devices.

wire-shaped supercapacitors, self-assembly, graphene fiber, high energy density, wearable electronics

Citation: Xiao P, Shi M J, Xu L, et al. An efficient chemical reduction-induced assembly of Fe_3O_4@graphene fiber for wire-shaped supercapacitors with ultrahigh volumetric energy density. Sci China Tech Sci, 2021, 64: 2246–2254, https://doi.org/10.1007/s11431-020-1896-5

1 Introduction

Integrating energy storage devices and textiles can satisfy the increasing demand for wearable electronics in recent years [1–3]. Conventional energy storage devices usually consist of inactive components such as rigid current collectors and insulating binder blocks, making them unable to meet the requirements for manufacturing wearable electronics [4–6]. Alternatively, the wire-shaped supercapacitors (SCs), which not only inherit the high power characteristics, rapid char-

*Corresponding authors (email: shiminjie@just.edu.cn; weifeng@tju.edu.cn)

ging-discharging process, long-term cycle life, high safety and environmentally benign of traditional SCs, but also could be utilized as fabrics directly in textiles, demonstrating great potentials in flexible electronic devices [6–8]. Although some progresses are achieved, the development of wire-shaped SCs is still limited by the low volumetric energy density, as well as the mutual restriction between electrochemical performance against their structural flexibility [9,10]. Accordingly, it remains challenging but becomes urgently needed for the exploration of high-performance wire-shaped SCs for portable/wearable electronics applications.

Due to the inherent advantages of low weight, tiny volume and high mechanical stability, various carbonaceous fiber-based linear electrodes have been proposed for wire-shaped SCs thus far [11–15], which could be integrated with textiles to produce wearable devices ensuring the maximum flexibility and wearability. Among them, graphene fiber (GF) holds great superiority to construct the wire-shaped SCs, which possesses the common merits of carbonaceous fibers such as excellent electrical conductivity and easy functionalization [16–20]. Extensive researches have been focused on the exploration of GF-based linear electrodes for wire-shaped SCs through integrating with the pseudocapacitive materials, such as MnO_2, WN, MoS_2, and $NiCo_2S_4$ [19–22]. Among all of the pseudocapacitive materials, Fe_3O_4 has become one of the highly desirable candidates for SCs due to its preferable electrical conductivity (~200 S cm^{-1}), high theoretical capacitance (~2299 F g^{-1}), abundant availability on earth and environmentally friendly [23–25]. Especially, it has multiple oxidation states of iron element, which can easily suffer from the reversible redox faradaic reaction in aqueous electrolyte [25,26]. However, almost no research has been reported on the design and preparation of graphene composite fiber using Fe_3O_4 as pseudocapacitive materials. Therefore, it is desirable to develop Fe_3O_4@GF composite linear electrode with enhanced electrochemical behaviors for wire-shaped SCs.

In this work, a novel flexible Fe_3O_4@GF composite linear electrode has been successfully synthetized via an efficient chemical reduction-induced assembly approach. When compared with common strategies such as the hydrothermal, chemical vapor deposition, and wet spinning. The experimental conditions of chemical reduction-induced assembly method are simple and mild for the preparation of GF-based linear electrode. Remarkably, the Fe_3O_4@GF composite linear electrode presents a robust fiber-shaped architecture, wherein the Fe_3O_4 nanoparticles (NPs) with a uniform size of ~10 nm effectively dispersed on the surface of graphene nanosheets without aggregation. In the composite structure, Fe_3O_4 NPs deliver their high pseudocapacitive characteristics, and exhibit strong surface adhesion to graphene nanosheets without affecting the softness and mechanical strength of linear electrode. Meanwhile, graphene nanosheets could serve as highly conductive path for rapid ion/electron transfer in the linear electrode, ensuring the excellent structural stability of Fe_3O_4 NPs during the charge-discharge cycles. Thanks to the well-designed composite architecture, the resultant Fe_3O_4@GF linear electrode possesses a considerable large volumetric specific capacitance (~250.75 F cm^{-3}), remarkable rate capability and electrochemical kinetics in aqueous electrolyte. Furthermore, a new type wire-shaped SC has been assembled by coupling the Fe_3O_4@GF linear electrode with gel electrolyte, which exhibit great flexibility and weavability, ultrahigh volume energy density (18.8 mWh cm^{-3}) and long-term cycling life (~93.5% retention over 10000 cycles), implying great values for future portable and wearable electronic applications.

2 Experimental procedure

2.1 Preparation of Fe_3O_4@GF

Graphene oxide (GO) was prepared from natural graphite (325 mesh, 99.8%) through modified Hummers method [27,28]. Fe_3O_4 NPs were synthesized by a simple chemical coprecipitation method [22]. GO aqueous solution and Fe_3O_4 NPs dispersion were mixed under ultrasonication for 30 min, wherein the mass ratio of Fe_3O_4 NPs and GO was controlled at about 80:20. Under stirring, 50 mg of ascorbic acid (VC) was sequentially added into the 20 mL above uniform dispersion (~4 mg mL^{-1}). The resulting mixed solution was then injected into several pipes with the diameter of 5 mm and sealed at both ends. After reacting at 85°C for 3 h, the glass pipes with open ends were dried in air at 50°C to obtain Fe_3O_4@GF. Finally, the Fe_3O_4@GF was heated at 200°C for 2 h under Ar atmosphere to remove the residual VC. For comparison, similar process was employed for the preparation of pristine GF without the addition of Fe_3O_4 NPs.

2.2 Assembly of the wire-shaped SC

For the fabrication of wire-shaped SC, the Fe_3O_4@GF and CNT@GF were utilized as negative and positive linear electrodes, respectively. The CNT@GF was obtained according to the previous literature [23]. Besides, PVA-KOH gel electrolyte was prepared with 6 g PVA, 3 g KOH, and 60 mL of deionized water. The Fe_3O_4@GF negative and CNT@GF positive linear electrodes were both immersed into the mixture solution for 10 min. After being taken out, two linear electrodes were completely encapsulated into the PVA-KOH gel electrolyte, which were then simply intertwined with each other. At this moment, two twined electrodes were further coated by slight gel electrolyte again to firmly assemble the wire-shaped SC.

2.3 Material characterization

Morphology of the Fe_3O_4@GF sample was observed by using emission scanning electron microscopy (SEM, FEI Sirion 200) working at 3.0 kV and Transmission electron microscope (TEM, JEM-2100F) working at 200 kV. Thermogravimetric analysis (TGA) of the Fe_3O_4@GF was performed on a SDT Q600 Build analyzer ranging from 20°C to 800°C at a heating rate of 5°C min^{-1} under air condition. Crystallinity and composition were investigated using power X-ray diffraction (XRD) pattern on a Bruker D8 Advance X-ray equipment with 2D detector (Cu K_α, λ=1.5406 Å), X-ray photoelectron spectroscopic (XPS) measurement realized by Kratos AXIS Ultra DLD spectrometer (Al Ka X-ray source). All the electrochemical measurements were carried out by using a VMP3 multifunctional electrochemical station (Bio-Logic, France) via common cyclic voltammetry (CV), galvanostatic charge-discharge (GCD), and electrochemical impedance spectroscopy (EIS) methods. The CV and GCD tests were systematically measured under various scan rates/current densities. The volumetric specific capacitance of wire-shaped SC and corresponding energy/power densities were calculated from the galvanostatic discharge curve based on the two-electrode calculation method as provided in the supplementary materials.

3 Results and discussion

The preparation procedure of Fe_3O_4@GF based on the chemical reduction-induced assembly is schematically illustrated in Figure 1(a). Initially, the mixed solution containing GO, Fe_3O_4 NPs and VC is injected into a glass pipe slowly. After sealing the both ends, the pipe is heated with a constant temperature of 85°C to conduct the reduction of GO. During the process, as the shrinkage of GO and the gases pressure generated by the decomposition of the functional groups on GO, the GO and Fe_3O_4 NPs tend to be slender pillar in the center of glass pipe, realizing the effective assembly with each other [17,18]. It should be noted that this process must be conducted in a closed reactor under a certain amount of pressure. If the two ends of the glass pipe are not fastened up fully, the resultant Fe_3O_4@GF could be easily scattered and fractured. Finally, two ends of the glass pipe are opened for further dry and then the fiber-shaped Fe_3O_4@GF is obtained

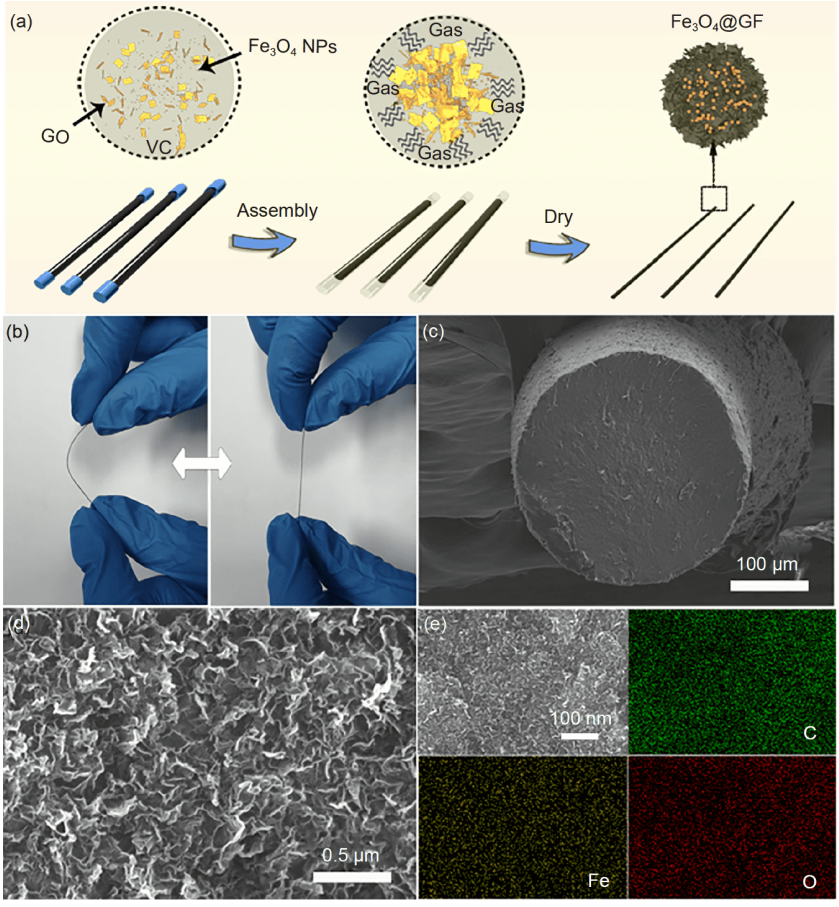

Figure 1 (Color online) (a) Schematic illustration of chemical reduction-induced assembly of Fe_3O_4@GF; (b) photographs of the Fe_3O_4@GF electrode with favorable flexibility and bendability; (c) and (d) SEM images captured in different magnifications and (e) the corresponding EDS (C, Fe, and O) elemental mapping images of the Fe_3O_4@GF.

(Figure 1(b)), wherein the interactions between Fe_3O_4 and GF are the electrostatic and van der Waals interactions. Owing to the interactions between Fe_3O_4 and GF, the Fe_3O_4@GF as linear electrode shows excellent long-term cycling performance with almost no structure evolution during charge/discharge cycles (Figure S1). Interestingly, the length and diameter of the as-prepared Fe_3O_4@GF could be controlled by changing the sizes of the used glass tube.

Figure 2(a) and (b) disclose a deep insight into the microscopic morphology of Fe_3O_4@GF by the TEM characterization. Notably, a large number of Fe_3O_4 NPs with a uniform size of ~10 nm anchored on the surface of graphene nanosheets (Figure 2(a)), indicating the effective assembly between the graphene nanosheets and Fe_3O_4 NPs. As the TEM image of Fe_3O_4 NPs shown, it is observed that the aggregation phenomenon of Fe_3O_4 NPs is extremely serious (Figure S2). By contrast, in the Fe_3O_4@GF composite structure, the Fe_3O_4 NPs are dispersed in the graphene nanosheets, while the aggregation of Fe_3O_4 NPs could be effectively relieved. Although there still exist some Fe_3O_4 NPs aggregation in the Fe_3O_4@GF composite fiber, it is undeniable that the introduction of graphene nanosheets can alleviate the serious aggregation of Fe_3O_4 NPs in a considerable extent. The high-resolution TEM (HRTEM) image (Figure 2(b)) displays clear lattice fringe with the crystal interplanar spacing of ~0.20 nm, corresponding to the (311) plane of cubic-

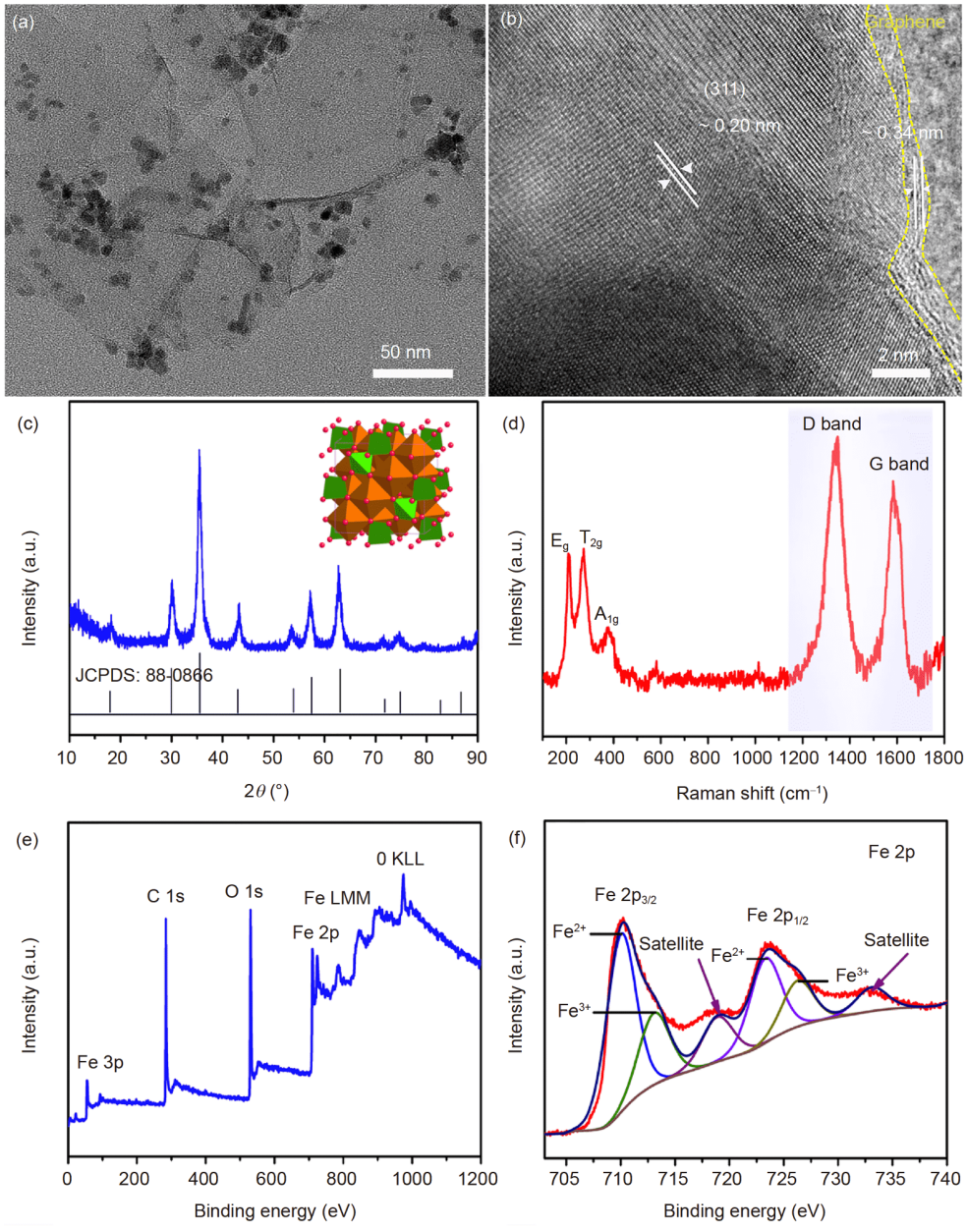

Figure 2 (Color online) (a) Typical TEM image and (b) the corresponding high-resolution TEM image of Fe_3O_4@GF; (c) XRD pattern, (d) Raman spectra, (e) XPS overall spectrum and (h) the Fe 2p high-resolution spectra of Fe_3O_4@GF.

spinel Fe_3O_4, while the edge region shows the lattice fringe of ~0.34 nm, which belongs to the (002) plane of graphene in the Fe_3O_4@GF. The XRD pattern can also confirm this result. As shown in Figure 2(c), typical characteristic peaks are assigned to the cubic spinel structural Fe_3O_4 (JCPDS no. 88-0866) [24], wherein these sharp diffraction peaks reveal the high crystallinity of Fe_3O_4 NPs. Nevertheless, there is no peak of graphene nanosheets in the XRD pattern, which is due to the low degree graphitization of graphene nanosheets with disordered stacking structure [25]. Raman spectra of Fe_3O_4@GF are observed in Figure 2(d). Clearly, apart from the D band (~1350 cm^{-1}) and G band (~1590 cm^{-1}) in relation with graphene nanosheets, the main Raman bands are located at 200–400 cm^{-1} for Fe_3O_4@GF, which are consistent with the main vibrational features (A_{1g} +E_g+T_{2g}) of cubic-spinel Fe_3O_4 [26,27]. In addition, the electronic state and elemental composition of Fe_3O_4@GF were analyzed by mean of XPS measurement. The overall survey spectrum (Figure 2(e)) indicates that the Fe_3O_4@GF only contains C, Fe and O atoms without other impurities. Figure 2(f) displays the XPS high-resolution spectra of Fe 2p, which are fitted with two spin-orbit doublets and two shakeup satellites. The doubles are the characteristic peaks of Fe^{2+} and Fe^{3+}, which are identical with previous reports [28,29]. According to the TGA measurements (Figure S3), the mass amount of Fe_3O_4 NPs in the Fe_3O_4@GF is determined to be about 72.1%.

The electrochemical behaviors of pristine GF and Fe_3O_4@GF as the linear electrode were evaluated using the three-electrode tested configuration in KOH aqueous electrolyte. As seen from Figure 3(a), the CV curve of the Fe_3O_4@GF linear electrode exhibits a couple of broad redox peaks located at about −0.85 V (cathodic peak) and −0.57 V (anodic peak), delivering a larger specific capacitance than pristine GF linear electrode with limited electric double-layer storage (rectangular-like CV curve). Figure 3(b) shows that the set of redox peaks could be observed for the cathodic/anodic sweeps in the CV curves scanning at various rates of the Fe_3O_4@GF linear electrode. This obvious pseudocapacitive storage is mainly related to the redox reaction: Fe(II)↔Fe(III) [30,31]. As for Fe_3O_4@GF linear electrode, apart from the GF possessing electric double-layer capacitance (EDLC), the pseudocapacitive behaviors are associated with the redox reaction of Fe_3O_4 NPs in the Fe_3O_4@GF linear electrode. The large specific capacitance of the Fe_3O_4@GF linear electrode is due to the synergistic effects of GF and Fe_3O_4 NPs. Both of the EDLC of GF and the pseudocapacitance of Fe_3O_4 NPs provide the favorable capacitive-storage performance for the Fe_3O_4@GF linear electrode in KOH aqueous electrolyte. Figure 3(c) presents the GCD curves of Fe_3O_4@GF linear electrode at different current densities, wherein the negligible "IR drop" is revealed in the discharging curve, indicating the Fe_3O_4@GF linear electrode with extremely low internal resistance. Moreover, the GCD curves are all nonlinear at various current densities, further evincing the existence of pseudocapacitive storage in the Fe_3O_4@GF linear electrode during electrochemical process. Consequently, it is believed that the significant enhancement of the capacitive performance for Fe_3O_4@GF linear electrode can be ascribed to the synergetic effects between the pseudocapacitance of Fe_3O_4 NPs and the double-layer capacitance of graphene nanosheets in Fe_3O_4@GF linear electrode. Figure 3(d) displays the volumetric specific capacitance under various current densities (250–4000mA cm^{-3}) of the Fe_3O_4@GF linear electrode in KOH aqueous electrolyte. Remarkably, the specific capacitance of the Fe_3O_4@GF linear electrode based on the total volume at a current density of 250 mA cm^{-3} can reach as high as 250.75 F cm^{-3}, considerably higher than most of GF-based linear electrodes previously reported, such as PANI@GF (204.2 F cm^{-3}) [32], Co_3O_4@GF (165.7 F cm^{-3}) [33], PPy@GF (107.2 F cm^{-3}) [34], MnO_2@GF (66.1 F cm^{-3}) [35] and MoS_2@GF (30 F cm^{-3}) [20]. When the current density increases to 4000 mA cm^{-3}, the specific capacitance still remains at 160.52 F cm^{-3}. The remarkable rate performance of Fe_3O_4@GF linear electrode is beneficial from the fiber-shaped architecture constructed by the highly conductive GF with Fe_3O_4 NPs, providing high connectivity for rapid charge transfer in the Fe_3O_4@GF linear electrode during the electrochemical process. Moreover, GF serves as the substrate to couple with Fe_3O_4 NPs, which effectively buffer the strain from volume change and inhibit the fusion of Fe_3O_4 NPs, rendering stability and integrity of the Fe_3O_4@GF linear electrode upon cycling. For comparison, the electrochemical behaviors of pristine Fe_3O_4 as electrode were provided in Figure S4.

EIS measurement is an effective way to study the electrochemical kinetic characteristics of SCs electrode. The EIS plot of Fe_3O_4@GF linear electrode has been carried out and displayed in Figure 3(e). The point where the high frequency region intersects the real axis represents the equivalent series resistance (R_s), which represents the total internal resistance of linear electrode. As observed in the inset of Figure 3(e), the R_s value of Fe_3O_4@GF linear electrode is determined as low as 0.52 Ω in return of its high electrical conductivity. In addition, in the high frequency region, the diameter of the semicircle is related with the charge transfer resistance (R_{ct}), and the linear part in the low frequency area represents the Warburg impedance (Z_w), that is, the diffusion impedance of electrolyte ions in the linear electrode. Obviously, the Fe_3O_4@GF linear electrode shows a very small semicircle and an almost vertical line, which indicates that the Fe_3O_4@GF linear electrode exhibits high electrochemical kinetics of charge transport and ionic diffusion.

Furthermore, it is well known that the total capacitive behavior of the SCs electrode originates from the non-dif-

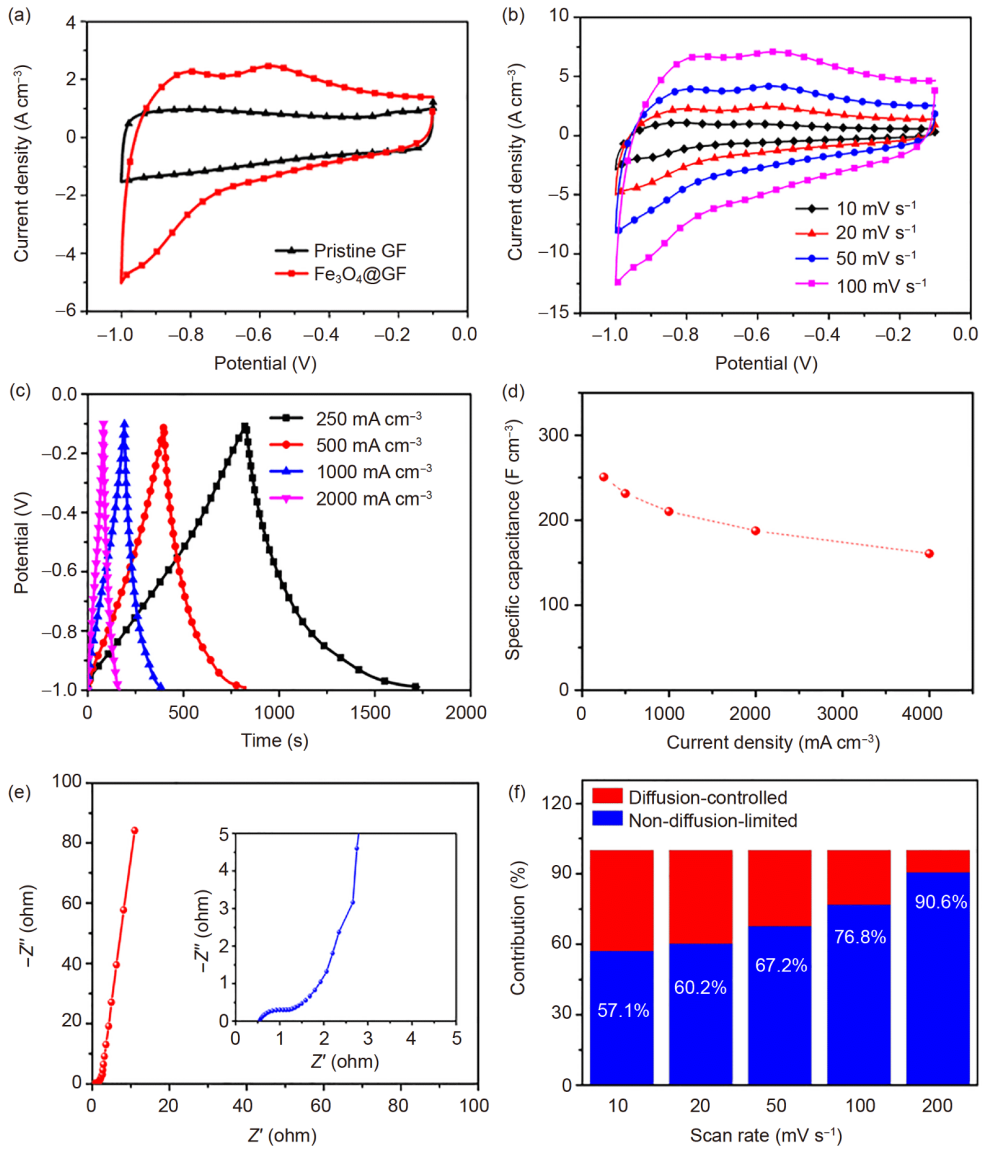

Figure 3 (Color online) (a) Comparison of CV curves scanning at 20 mV s^{-1} of pristine GF and Fe_3O_4@GF linear electrodes in KOH aqueous electrolyte; (b) CV curves scanning at various rates, (c) GCD curves under various current densities, (d) volumetric specific capacitance at different current densities, (e) EIS plot and (f) the capacitance contribution at various scan rates of the Fe_3O_4@GF linear electrode in 2 M KOH aqueous electrolyte.

fusion-limited process and diffusion-controlled process, which can be quantified by the previous reported equation [36,37]. It is found that the non-diffusion-limited storage is prominent in the Fe_3O_4@GF linear electrode (Figure 3(f)), revealing that the redox reaction is caused by the fast pseudocapacitive process rather than the slow diffusion-controlled battery-like energy storage [37,38]. Based on the above discussion, the resultant Fe_3O_4@GF linear electrode not only shows high mechanical stability with excellent flexibility, but also exhibits large specific capacitance, high electrochemical kinetics and remarkable rate capability in aqueous electrolyte.

As a proof of concept, a novel wire-shaped SC using gel electrolyte (PVA-KOH) was assembled, for which Fe_3O_4@GF and CNT@GF served as the negative and positive linear electrodes, respectively (Figure 4(a)). The fabricated wire-shaped SC exhibits a high degree of flexibility, mechanically stability and bendability without disrupting the electrochemical behaviors (Figure S5). In order to further investigate the mechanical strength and electrochemical reliability of the wire-shaped SC, the assembled device was subsequently subjected to electrochemical behaviors under bending measurements. As shown in Figure S6, the CV curves under different bent degrees (i.e., 0°, 60°, and 120°) exhibit similar capacitive-storage behavior to that of the straight state, which indicates that wire-shaped SC exhibits high electrochemical reliability and all-round flexibility. Profiting from the soft and supple device structure, the wire-shaped SC can be readily woven into the cloths (Figures 4(b) and S7). Importantly, wire-shaped SC is able to successfully

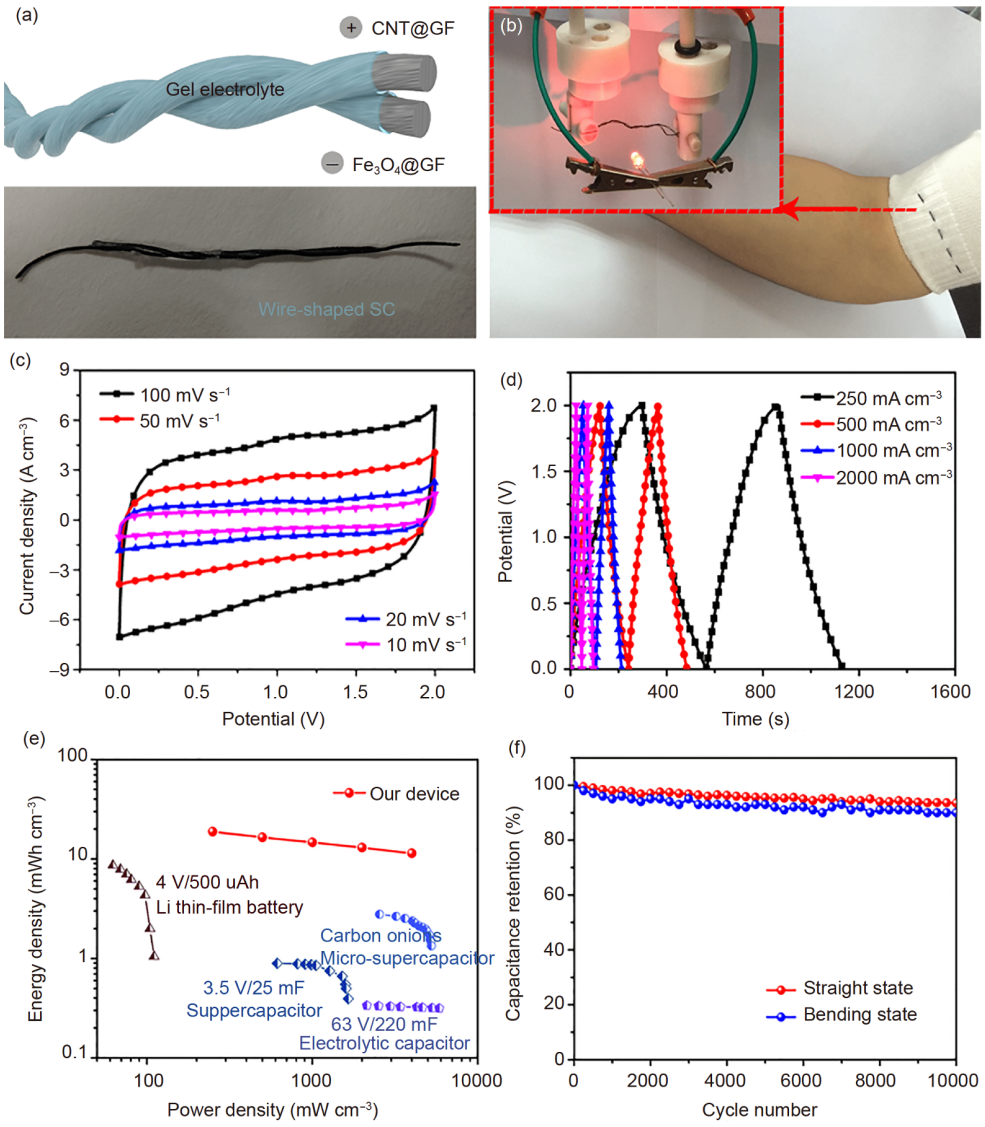

Figure 4 (Color online) (a) Schematic illustration and photograph of the flexible wire-shaped SC based on Fe_3O_4@GF and CNT@GF linear electrodes; (b) The wire-shaped SC woven in a real clothing and its efficient energy storage capacity; (c) CV curves at the scan rates (10–100 mV s^{-1}) and (d) GCD curves at the current densities (100–800 mA cm^{-3}) of the wire-shaped SC; (e) ragone plot of wire-shaped SC compared with the commercial energy storage devices. (f) long-term cycling stabilities of the wire-shaped SC under straight/bending states after 10000 cycles.

drive the light-emitting-diode (LED) (inset in Figure 4(b)), indicating the remarkable power supply of the wire-shaped SC as suitable energy storage device. Figure 4(c) exhibits the CV curves of the wire-shaped SC measured with scan rates from 10 to 100 mV s^{-1}. All CV curves present almost no distortion when increasing the sweep rates in the range from 0 to 2.0 V, indicating the efficient ion/electron transportation of assembled devices. According to the GCD curves under different current densities, the volume energy and power densities of the wire-shaped SC can be calculated, and their relationship is depicted using the ragone plots. As observed in Figure 4(e), the wire-shaped SC can provide a considerably high volumetric capacitance of 33.8 F cm^{-3}, and the maximum volumetric energy density can reach as high as 18.8 mWh cm^{-3} (87.2 μWh cm^{-2}), which is much superior to reported wire/fiber-shaped SCs, such as wire-shaped SCs based on poly(ionic liquid)/GF (8.28 mWh cm^{-3}) [39], CNT/GF (36 μWh cm^{-2}) [40], MnO_2/carbon fiber (30.2 μWh cm^{-2}) [41], activated carbon felts (35.6 μWh cm^{-2}) [42] and so on (Table S1), dozens of higher than that of commercial SCs (3.5 V/35 mF, <1 mWh cm^{-3}), and even twice higher than that of available 4 V/500 μAh Li-ion thin-film batteries (~10 mWh cm^{-3}) [43,44]. At the same time, the maximum volumetric power density of wire-shaped SC can reach up to 4000 mW cm^{-3}, which is equivalent to that of commercial commercially available SCs [40]. Furthermore, the cycling performances of wire-shaped SC under the straight and bending states have been also measured. As seen from Figure 4(f), the long-term cycling stabilities both exhibit the considerably high retention about 93.5% and 90.2% over 10000

charging-discharging cycles. Therefore, the fabricated wire-shaped SC provides a great possibility to meet the diverse needs for highly efficient energy storage in portable/wearable electronics applications.

4 Conclusions

Summarily, a novel Fe_3O_4@GF linear electrode with omnidirectional flexibility and high electrochemical activity has been successfully prepared through an efficient chemical reduction-induced assembly. The synergy of electrochemically active Fe_3O_4 NPs and conductive graphene nanosheets endows the linear electrode with improved electric conductivity, boosted charge-transfer kinetics and enhanced structural integrity. Hence, the Fe_3O_4@GF linear electrode exhibits a large volumetric specific capacitance of ~250.75 F cm^{-3}, excellent rate capability and favorable electrochemical kinetics in aqueous electrolyte, which is superior than reported GF-based linear electrodes. For real application, a kind of wire-shaped SCs based on Fe_3O_4@GF linear electrode also has been fabricated, delivering ultrahigh volumetric energy density of 18.8 mWh cm^{-3} and excellent performance stability at various deformation states. Prospectively, this work can enlighten the preparation and application of GF-based linear electrode that can be applied to high-performance portable and wearable devices.

This work was supported by the National Natural Science Foundation of China (Grant Nos. 61904116, 52002157), the Natural Science Foundation of Jiangsu Province (Grant No. BK20190976), and the Science and Technology Project of State Grid Corporation of China (Grant No. 5455DW190009).

Supporting Information

The supporting information is available online at tech.scichina.com and link.springer.com. The supporting materials are published as submitted, without typesetting or editing. The responsibility for scientific accuracy and content remains entirely with the authors.

1 Chen X, Villa N S, Zhuang Y, et al. Stretchable supercapacitors as emergent energy storage units for health monitoring bioelectronics. Adv Energy Mater, 2020, 10: 1902769
2 Shang J, Huang Q Y, Wang L, et al. Soft hybrid scaffold (SHS) strategy for realization of ultrahigh energy density of wearable aqueous supercapacitors. Adv Mater, 2020, 32: 1907088
3 Zhu Q, Zhao D, Cheng M, et al. A new view of supercapacitors: Integrated supercapacitors. Adv Energy Mater, 2019, 9: 1901081
4 Sun H, Zhang Y, Zhang J, et al. Energy harvesting and storage in 1D devices. Nat Rev Mater, 2017, 2: 17023
5 Yang M, Xia H. Exploration and progress of high-energy supercapacitors and related electrode materials. Sci China Tech Sci, 2015, 58: 1851–1863
6 Chen D, Jiang K, Huang T T, et al. Recent advances in fiber supercapacitors: Materials, device configurations, and applications. Adv Mater, 2020, 32: 1901806
7 Wang S, Liu N, Su J, et al. Highly stretchable and self-healable supercapacitor with reduced graphene oxide based fiber springs. ACS Nano, 2017, 11: 2066–2074
8 Liao M, Ye L, Zhang Y, et al. The recent advance in fiber-shaped energy storage devices. Adv Electron Mater, 2019, 5: 1800456
9 Chen S, Wang L, Huang M, et al. Reduced graphene oxide/Mn_3O_4 nanocrystals hybrid fiber for flexible all-solid-state supercapacitor with excellent volumetric energy density. Electrochim Acta, 2017, 242: 10–18
10 Zhang J, Yang X, He Y, et al. δ-MnO_2 /holey graphene hybrid fiber for all-solid-state supercapacitor. J Mater Chem A, 2016, 4: 9088–9096
11 Tebyetekerwa M, Marriam I, Xu Z, et al. Critical insight: Challenges and requirements of fibre electrodes for wearable electrochemical energy storage. Energy Environ Sci, 2019, 12: 2148–2160
12 Wang C, Hu K, Li W, et al. Wearable wire-shaped symmetric supercapacitors based on activated carbon-coated graphite fibers. ACS Appl Mater Interfaces, 2018, 10: 34302–34310
13 Wang L, Liu R. Knitting controllable oxygen-functionalized carbon fiber for ultrahigh capacitance wire-shaped supercapacitors. ACS Appl Mater Interfaces, 2020, 12: 44866–44873
14 Xu P, Wei B, Cao Z, et al. Stretchable wire-shaped asymmetric supercapacitors based on pristine and MnO_2 coated carbon nanotube fibers. ACS Nano, 2015, 9: 6088–6096
15 Ma W, Chen S, Yang S, et al. Flexible all-solid-state asymmetric supercapacitor based on transition metal oxide nanorods/reduced graphene oxide hybrid fibers with high energy density. Carbon, 2017, 113: 151–158
16 Fang B, Chang D, Xu Z, et al. A review on graphene fibers: Expectations, advances, and prospects. Adv Mater, 2020, 32: 1902664
17 Li J, Li J, Li L, et al. Flexible graphene fibers prepared by chemical reduction-induced self-assembly. J Mater Chem A, 2014, 2: 6359–6362
18 Qu G, Cheng J, Li X, et al. A fiber supercapacitor with high energy density based on hollow graphene/conducting polymer fiber electrode. Adv Mater, 2016, 28: 3646–3652
19 Zhu H, An Y, Shi M, et al. Porous N-doped carbon/MnO_2 nanoneedles for high performance ionic liquid-based supercapacitors. Mater Lett, 2021, 296: 129837
20 Sun G, Liu J, Zhang X, et al. Fabrication of ultralong hybrid microfibers from nanosheets of reduced graphene oxide and transition-metal dichalcogenides and their application as supercapacitors. Angew Chem Int Ed, 2014, 53: 12576–12580
21 Salman A, Sasikala S P, Kim I H, et al. Tungsten nitride-coated graphene fibers for high-performance wearable supercapacitors. Nanoscale, 2020, 12: 20239–20249
22 Cai W, Lai T, Lai J, et al. Transition metal sulfides grown on graphene fibers for wearable asymmetric supercapacitors with high volumetric capacitance and high energy density. Sci Rep, 2016, 6: 26890
23 Mondal S, Rana U, Malik S. Reduced graphene oxide/Fe_3O_4/polyaniline nanostructures as electrode materials for an all-solid-state hybrid supercapacitor. J Phys Chem C, 2017, 121: 7573–7583
24 Zeng Y, Yu M, Meng Y, et al. Iron-based supercapacitor electrodes: Advances and challenges. Adv Energy Mater, 2016, 6: 1601053
25 Sheng S, Liu W, Zhu K, et al. Fe_3O_4 nanospheres *in situ* decorated graphene as high-performance anode for asymmetric supercapacitor with impressive energy density. J Colloid Interface Sci, 2019, 536: 235–244
26 Nawwar M, Poon R, Chen R, et al. High areal capacitance of Fe_3O_4-decorated carbon nanotubes for supercapacitor electrodes. Carbon Energy, 2019, 1: 124–133
27 Yang Z, Qian K, Lv J, et al. Encapsulation of Fe_3O_4 nanoparticles into N, S co-doped graphene sheets with greatly enhanced electrochemical performance. Sci Rep, 2016, 6: 27957
28 Pan L, Zhu X D, Xie X M, et al. Smart hybridization of TiO_2 nanorods and Fe_3O_4 nanoparticles with pristine graphene nanosheets: Hierarchically nanoengineered ternary heterostructures for high-rate lithium storage. Adv Funct Mater, 2015, 25: 3341–3350
29 Wang X, Liu Y, Arandiyan H, et al. Uniform Fe_3O_4 microflowers hierarchical structures assembled with porous nanoplates as superior

anode materials for lithium-ion batteries. Appl Surf Sci, 2016, 389: 240–246
30 Wang Q, Jiao L, Du H, et al. Fe_3O_4 nanoparticles grown on graphene as advanced electrode materials for supercapacitors. J Power Sources, 2014, 245: 101–106
31 Lin T W, Dai C S, Hung K C. High energy density asymmetric supercapacitor based on NiOOH/Ni_3S_2/3D graphene and Fe_3O_4/graphene composite electrodes. Sci Rep, 2015, 4: 7274
32 Liu D, Liu J, Wang Q, et al. PANI coated microporous graphene fiber capable of subjecting to external mechanical deformation for high performance flexible supercapacitors. Carbon, 2019, 143: 147–153
33 Wang W, Yuan Y, Yang J, et al. Hierarchical core-shell Co_3O_4/graphene hybrid fibers: Potential electrodes for supercapacitors. J Mater Sci, 2018, 53: 6116–6123
34 Ding X, Zhao Y, Hu C, et al. Spinning fabrication of graphene/polypyrrole composite fibers for all-solid-state, flexible fibriform supercapacitors. J Mater Chem A, 2014, 2: 12355–12360
35 Ma W, Chen S, Yang S, et al. Hierarchical MnO_2 nanowire/graphene hybrid fibers with excellent electrochemical performance for flexible solid-state supercapacitors. J Power Sources, 2016, 306: 481–488
36 Shi M, Wang B, Shen Y, et al. 3D assembly of MXene-stabilized spinel $ZnMn_2O_4$ for highly durable aqueous zinc-ion batteries. Chem Eng J, 2020, 399: 125627
37 Wang X, Mathis T S, Li K, et al. Influences from solvents on charge storage in titanium carbide MXenes. Nat Energy, 2019, 4: 241–248
38 Zhou J, Yu J, Shi L, et al. A conductive and highly deformable all-pseudocapacitive composite paper as supercapacitor electrode with improved areal and volumetric capacitance. Small, 2018, 14: 1803786
39 Gopalsamy K, Yang Q, Cai S, et al. Wet-spun poly(ionic liquid)-graphene hybrid fibers for high performance all-solid-state flexible supercapacitors. J Energy Chem, 2019, 34: 104–110
40 Yang Z, Jia Y, Niu Y, et al. One-step wet-spinning assembly of twisting-structured graphene/carbon nanotube fiber supercapacitor. J Energy Chem, 2020, 51: 434–441
41 Li H, Liang J, Li H, et al. Activated carbon fibers with manganese dioxide coating for flexible fiber supercapacitors with high capacitive performance. J Energy Chem, 2019, 31: 95–100
42 Zhao Z, Wang X, Yao M, et al. Activated carbon felts with exfoliated graphene nanosheets for flexible all-solid-state supercapacitors. Chin Chem Lett, 2019, 30: 915–918
43 Chen G, Ai Y, Mugaanire I T, et al. A simple inorganic hybrids strategy for graphene fibers fabrication with excellent electrochemical performance. J Power Sources, 2020, 450: 227637
44 Zhou X, Qin Y, He X, et al. $Ti_3C_2T_x$ Nanosheets/$Ti_3C_2T_x$ quantum dots/RGO (reduced graphene oxide) fibers for an all-solid-state asymmetric supercapacitor with high volume energy density and good flexibility. ACS Appl Mater Interfaces, 2020, 12: 11833–11842